Macromolecules

Article

pubs.acs.org/Macromolecules

Incorporation of Fluorine onto Different Positions of Phenyl Substituted Benzo[1,2-*b*:4,5-*b*′]dithiophene Unit: Influence on Photovoltaic Properties

Jun Yuan,[†] Yingping Zou,*[,†,‡] Ruili Cui,[†] Yi-Hsiang Chao,[⊥] Zaiyu Wang,[∥] Mingchao Ma,[§] Yuehui He,[‡] Yongfang Li,[#] Amanda Rindgen,[¶] Wei Ma,*[,∥] Dequan Xiao,[¶] Zhishan Bo,[▽] Xinjun Xu,[§] Lidong Li,[§] and Chain-Shu Hsu*[,⊥]

[†]College of Chemistry and Chemical Engineering, Central South University, Changsha, 410083, China

[‡]State Key Laboratory for Powder Metallurgy, Central South University, Changsha, 410083, China

[⊥]Department of Applied Chemistry, National Chiao Tung University, Hsinchu, 30010, Taiwan

[∥]State Key Laboratory for Mechanical Behavior of Materials, Xi'an Jiaotong University, Xi'an 710049, China

[§]School of Materials Science and Engineering, University of Science and Technology Beijing, Beijing 100083, China

[#]Institute of Chemistry, Chinese Academy of Sciences, Beijing 100190, China

[¶]Department of Chemistry and Chemical Engineering, University of New Haven, West Haven, Connecticut 06516, United States

[▽]Beijing Key Laboratory of Energy Conversion and Storage Materials, Beijing Normal University, College of Chemistry, Beijing, 100875, China

S *Supporting Information*

ABSTRACT: We have designed and synthesized two low bandgap conjugated copolymers containing alternating *meta*-fluoro-*p*-alkoxyphenyl- (*m*-FPO-) or *p*-fluoro-*m*-alkoxyphenyl- (*p*-FPO-) substituted benzodithiophenes-*co*-benzooxadiazole (BO), named PBO-*m*-FPO and PBO-*p*-FPO. The properties, including UV−vis absorption, charge mobility and photovoltaic performance of the two polymers have been intensively investigated. The results indicated that the introduction of fluorine atom at *m*, *p* positions of phenyl substituted benzodithiophene unit hardly affected their absorption spectra and highest occupied molecular orbital (HOMO) level. However, the two polymers showed different photovoltaic properties. Power conversion efficiencies (PCEs) based on the device structure of ITO/PEDOT:PSS/polymer:$PC_{71}BM$/Ca/Al demonstrated a large distinction (5.9% for PBO-*m*-FPO vs 2.8% for PBO-*p*-FPO) at optimal weight ratio. When replacing the Ca layer with zirconium acetylacetonate (ZrAcac), using 3% 1,8-diiodooctane (DIO) as the active layer additive, the PCEs of PBO-*m*-FPO and PBO-*p*-FPO increased by 36% (8.0% vs 5.9%) and 85% (5.1% vs 2.8%), respectively. The active layer's mobilities, morphology and molecular packing resulted in a significant difference in short-circuit current density (J_{sc}) and fill factor (FF).

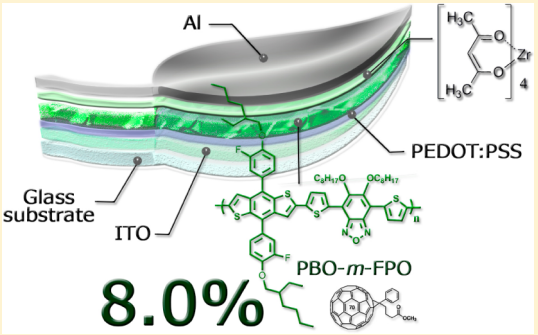

INTRODUCTION

Polymer solar cells (PSCs) based on bulk heterojunction (BHJ) have made tremendous advances toward commercialization.[1] Recently, the power conversion efficiencies (PCEs) of several polymers with single junction device have reached 11%.[2−5] As impressive and important renewable energy sources, PSCs have particular advantages such as simple device structure, lightweight, flexibility and low fabrication cost using simple ambient-condition solution or the roll-to-roll coating process.[6−8] Compared to inorganic-based solar cells, however, they still do not achieve the targeted 15% efficiency and satisfying lifetime, which is required for widespread commercialization.[9] Although optimizing the device fabrication[10,11] will improve photovoltaic performance, a promising candidate polymer with simple synthesis process is extremely in demand for broad applications of PSCs.[12]

For high-performance PSCs, the ideal strategy is to design donor−acceptor (D−A) alternating molecular structure for BHJ solar cell, which can offer the unique feature of tuning the energy levels and the bandgap.[13] As well-known, PCE is proportional to the open-circuit voltage (V_{oc}), short-circuit current density (J_{sc}), and fill factor (FF). So we can independently modulate D−A copolymers to obtain a low-lying the highest occupied molecular orbital (HOMO) energy

Received: March 17, 2015
Revised: June 6, 2015
Published: July 2, 2015

DOI: 10.1021/acs.macromol.5b00564
Macromolecules 2015, 48, 4347−4356

Scheme 1. Chemical Structures of PBO-*m*-FPO and PBO-*p*-FPO

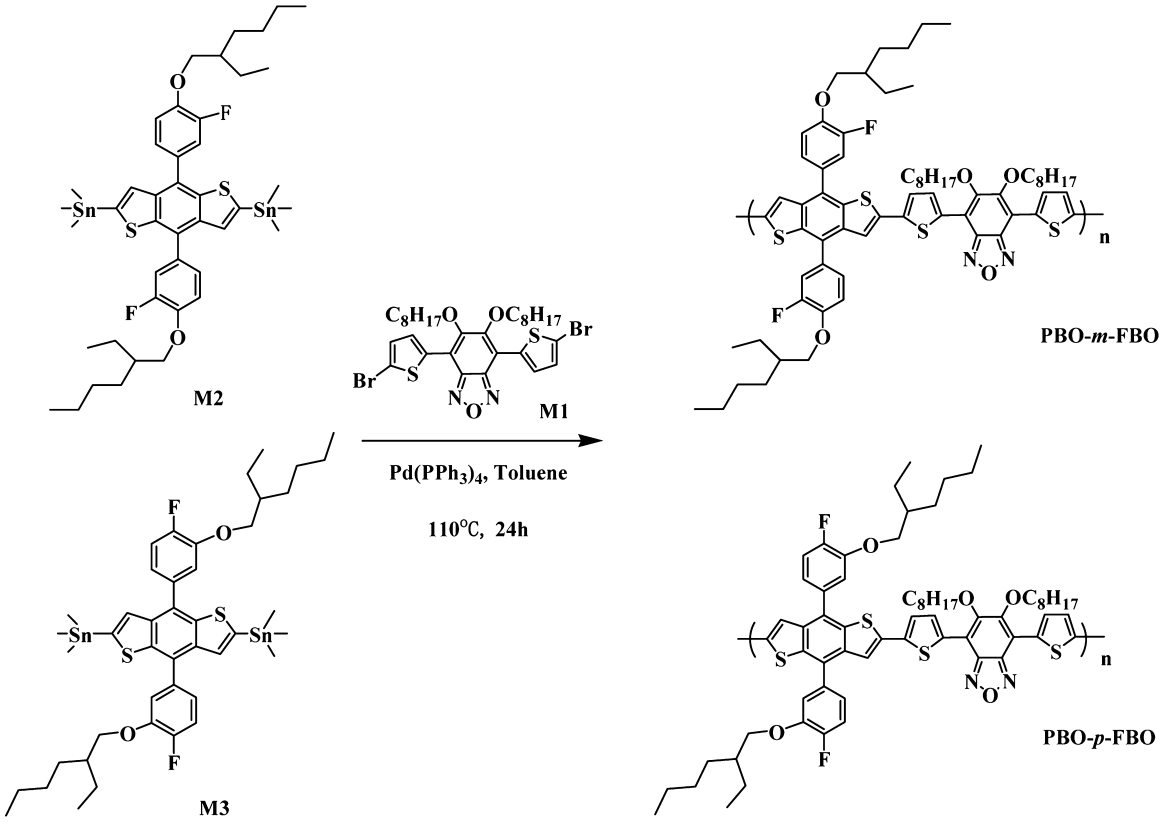

level to ensure a high V_{oc} and increase harvesting solar radiation efficiently to maximize J_{sc}.[14,15] Recently, the introduction of fluorine atoms into a polymer chain has shown great promise in enhancing PCEs of BHJ PSCs.[16−22] Fluorine is the strongest electron-withdrawing element with Pauling electronegative of 4.0 and a van der Waals radius of 1.35 Å, which may lower the HOMO energy levels resulting in some enhancement in V_{oc}. Meanwhile, fluorine substituted on a conjugated chain, not only minimizes any undesired steric hindrance but also can drastically alter the morphology of the active layer. Strong C−F···H and F···S interaction can occur to inter- and intramolecular, leading to smaller chain distance and a more face-on orientation, which can improve the polymer's charge mobility, resulting in a higher J_{sc} and FF.[23−25] According to the You's reported results, introduction of fluorine onto the periphery of the electron-acceptor (A) can increase PCEs of copolymers effectively.[26] When fluorine was attached to the electron-donor (D), however, the presence of a higher degree of exciton recombination, results in a poor photovoltaic performance.[27] Very recently, Hou and co-workers have added the fluorine to the 4,8-bis(thiophene-2-yl)-benzo[1,2-*b*:4,5-*b*′]dithiophene(BDT-T) unit, the V_{oc} of which is greatly improved by decreasing HOMO energy levels of D−A polymers without losing J_{sc} and FF.[28] Although fluorine substitution in the D−A polymers has made great success, the positions where it was placed remain interesting in investigating new photovoltaic polymers.[29] It is still unclear completely how the fluorine influences the optoelectronic properties.

Recently, our group reported the copolymerization of 4,7-di(5-bromothien-2-yl)-5,6-dioctyloxy benzo[c][1,2,5]-oxadiazole (M1)[30,31] with alkoxylphenyl substituted benzo-[1,2-*b*:4,5-*b*′]dithiophene- (BDT-) based (BDTPO), namely PBDTPO−DTBO, which provided a PCE of 6.2%.[32] As our previous results indicated, the electron-donor (BDTPO) moiety can reduce HOMO and lowest unoccupied molecular orbital (LUMO) energy level simultaneously, and the alkoxylphenyl group can effectively minimize torsional angles within polymer backbones, which will enhance the coplanarity.[33] Waston et al. found that the intramolecular interactions between F···S (in thiophene) via the noncovalent attractive could promote self-assembly and crystallinity of polymers.[24,34,35] Furthermore, fluorinated organic molecules could lead to better compatibility between donor and acceptor phases to shape highly ordered film morphology.[10] In order to carefully explore the effects of different positions of the fluorine atom and alkoxy group, using PBDTPO−DTBO as a model system, *m*-fluoro-*p*-alkoxyphenyl- and *p*-fluoro-*m*-alkoxyphenyl-substituted D−A polymers, PBO-*m*-FPO and PBO-*p*-FPO, were designed and synthesized (as shown in Scheme 1). Both of them showed good solubility in common organic solvents, similar optical and electrochemical properties. Interestingly, under the illumination of AM 1.5, 100 mW cm^{-2}, the PCEs of PBO-*m*-FPO and PBO-*p*-FPO based conventional BHJ solar cells demonstrated a drastic difference (7.3% vs 4.3%) using Ca/Al as cathodes after 3% DIO treatment at optimized weight ratios. Furthermore, using zirconium acetylacetonate (ZrAcac) as interlayer between the active layer and Al, higher PCEs of 8.0% and 5.1% were obtained for PBO-*m*-FPO and PBO-*p*-FPO, respectively.

RESULTS AND DISCUSSION

Material Synthesis. As shown in Scheme 1, the polymers PBO-*m*-FPO and PBO-*p*-FPO were synthesized by Stille

DOI: 10.1021/acs.macromol.5b00564
Macromolecules 2015, 48, 4347−4356

coupling reactions with $Pd(PPh_3)_4$ as a catalyst in toluene. The detailed synthetic procedures were described in Supporting Information. They were carefully purified by continuous Soxhlet extractions with methanol, hexane, and $CHCl_3$. Then $CHCl_3$ fraction was concentrated under vacumm evaporation, precipitated into methanol and collected by filtration. The number-average molecular weights (M_n) of PBO-*m*-FPO and PBO-*p*-FPO are 12 kDa and 15 kDa with corresponding polydisperse indices (PDIs) of 2.6 and 2.1. Thermal stability of the polymers was analyzed by thermogravimetric analysis (TGA); PBO-*m*-FPO and PBO-*p*-FPO possess good thermal stability with decomposition temperatures (5% weight loss) of 303 and 310 °C under an inert atmosphere, respectively (Figure S7). The molecular weights and thermal data for the polymers are shown in Table 1. The calculated bond angles (θ)

Table 1. Molecular Weight and Thermal Properties of the Copolymers

polymers	M_n (kDa)	PDI	yield (%)	T_d (°C)
PBO-*m*-FPO	12.3	2.6	35	303
PBO-*p*-FPO	1.53	2.1	66	310

were summarized in Table 2. θ_1, θ_2, θ_3, θ_4 and θ_5 are the inter- and interannual twisted angle. As can be seen from Table 2, the calculation results indicate an almost orthogonal configuration of the top/bottom phenyl to the center benzene in benzodithiophene. Such a "separation" of the top/bottom phenyls from the benzodithiophene, in terms of electronic/optical/extended conjugation, would minimize any impact these top/bottom phenyls would have on the benzodithiophene.

Optical Properties. UV−vis absorption spectra of polymers in chlorobenzene (CB) solution and thin film are shown in Figure 1 and the characteristics of the polymers absorption are listed in Table S1 (Supporting Information. Both polymers show similar absorption peaks in solution from 350 to 700 nm, which may be attributed to the localized $\pi-\pi$ and internal charge transfer transitions (ICT), respectively. Furthermore, the polymers in CB at 90 °C showed similar UV−vis profiles, where the spectra are blue-shifted compared with those at room temperature, which indicated a little aggregation of polymer backbone at room temperatures. Meanwhile, a similar red-shift of about 40 nm for the films of PBO-*m*-FPO and PBO-*p*-FPO was found when compared to those from solution state, indicating that there exist strong $\pi-\pi$ interaction peaks in both polymer films. From the onset (λ_{edge}) of both polymers' thin films, the optical band gaps ($E_g^{opt} = 1240/\lambda_{edge}$) of 1.64 and 1.66 eV were obtained for PBO-*m*-FPO and PBO-*p*-FPO, respectively. It is worthy to note that the absorption spectra and optical bandgaps of the polymers were very similar to the reported nonfluorinated polymer−PBDTPO−DTBO.[32]

Electrochemical Properties. HOMO and LUMO levels of two polymers were investigated by cyclic voltammetry (CV), and CV curves are shown in Figure 2. The HOMO energy level of polymers can be calculated according to the following equation $E_{HOMO} = -(E_{ox} + 4.4)$ (eV), where the unit of E_{ox} is in V vs. Ag/AgCl. The HOMO level of PBO-*m*-FPO and PBO-*p*-FPO were −5.53 and −5.54 eV, respectively. The LUMO energy level was calculated from the difference between the HOMO energy level and the optical bandgap.[36]

In order to further understand the electronic properties of the polymers, we used the NWChem program package[37] for all of the calculations. We used the density functional theory method at the B3LYP/6-31G* level. DFT/B3LYP/6-31G* has been found to be an accurate method to calculate the optimal geometry and electronic structures of many molecular systems. To simplify the calculations, all the alkyl chains of the polymer units were replaced by $-CH_3$ groups. Figure S8 shows that the molecular geometries and electronic wave function distribution of the HOMO and LUMO of the D−π−A model compounds. For the two polymers, the electronic wave function of the HOMO was distributed entirely over the conjugated molecules, which is beneficial for obtaining higher hole mobility.[38] The electronic wave function of the LUMO was mainly localized on the electron accepting part. From the DFT level calculations combined with equations provided by Leclerc group,[39] HOMO and LUMO energy levels of PBO-*m*-FPO and PBO-*p*-FPO are calculated to be −5.49 and −3.65 eV and −5.48 and −3.64 eV, respectively, which are quantitatively in agreement with the observed experimental results that *m*-/*p*- positions of the fluorine atom could trivially affect the electronic and optical properties of the copolymers in this system. The similar HOMO and LUMO levels of two polymers may originate from the side chain separated from the backbone by a benzene unit, which can be in agreement with the calculation results.

Photovoltaic Properties. To compare the photovoltaic properties, the conventional configuration devices were fabricated based on two polymers (Figure 3c). Usually, the low workfunction materials, such as Ca, were used to engineer

Table 2. Calculated Bond Angles of the Repeat Units of the Copolymers[a]

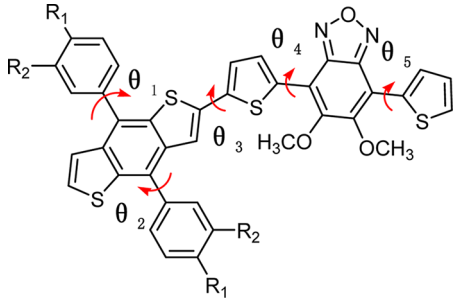

	R	θ_1 (deg)	θ_2 (deg)	θ_3 (deg)	θ_4 (deg)	θ_5 (deg)
PBO-*m*-FPO	$R_1 = OCH_3$; $R_2 = F$	82.6	70.1	35.1	55	41.1
PBO-*p*-FPO	$R_1 = F$; $R_2 = OCH_3$	78.8	72.1	37.5	64	79.6

[a]Illustration of θ1, θ2, θ3, θ4, and θ5 is given in graphic.

DOI: 10.1021/acs.macromol.5b00564
Macromolecules 2015, 48, 4347−4356

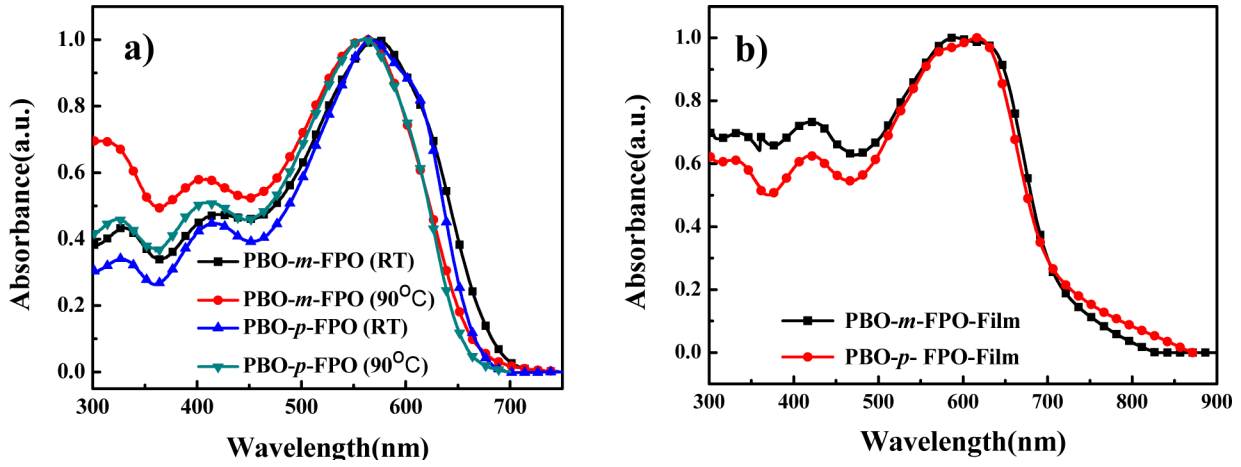

Figure 1. UV−vis absorption spectra of PBO-*m*-FPO and PBO-*p*-FPO: (a) solutions in dilute chlorobenzene at room temperature and 90 °C; (b) films on quartz cast from chloroform solution.

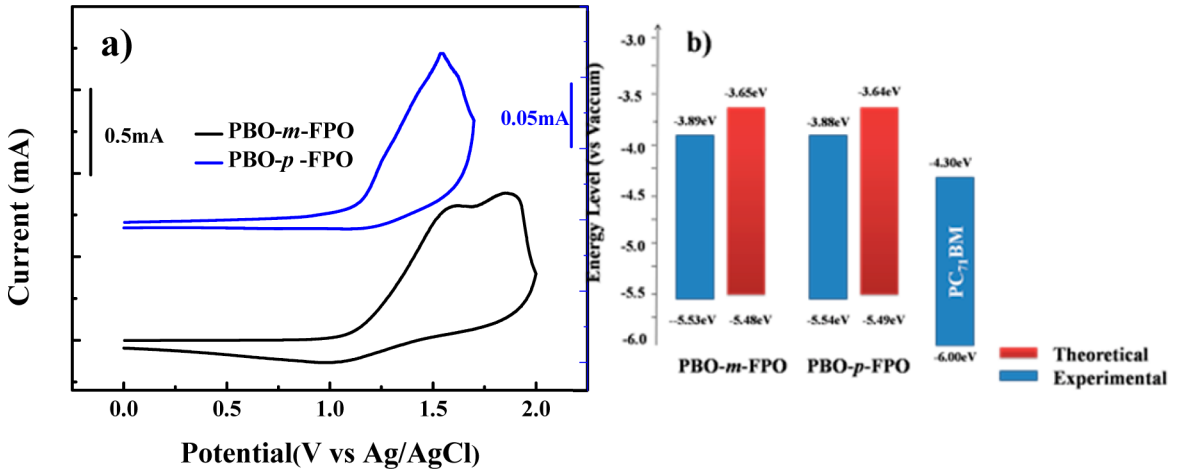

Figure 2. (a) Cyclic voltammograms of polymer films on a glassy carbon electrode in 0.1 M Bu_4NPF_6, CH_3CN solution. (b) Theoretical and experimental energy levels of polymers from CV measurements and DFT calculations.

the interface between the active layer and the cathode, forming ohmic contact with active layer and improving electron extraction.[40] However, the degradation is ubiquitous in PSCs since oxidation of the interlayer metals, preventing the commercialization of PSCs. Recently, Tan and co-workers reported alcohol/water-solution material, ZrAcac, as the interlayer spin-coated on the photoactive layer, which show decreased series resistance and enhanced photocurrent, resulting in remarkable improvement of PCEs.[41] Herein, the active layers were finally spin-coated from the polymers/$PC_{71}BM$ in orth-dichlorobenzene (ODCB). Figure 3a shows the current density versus voltage (J−V) characteristic curves of the best PSCs with Ca or ZrAcac as interlayer between the photosensitive layers and Al cathode under the illumination of AM 1.5, 100 mW cm^{-2}. While the device with Ca as cathode interlayer, the optimal D/A weight ratio of the PBO-*m*-FPO:$PC_{71}BM$ was found to be 1:2, exhibiting a PCE of 5.9% with V_{oc} = 0.89 V, J_{sc} = 11.3 mA cm^{-2}, and FF = 58%. By adding the high boiling point as additive (3% vol DIO), V_{oc} showed a little difference. Surprisingly, PCE of the PSC based on PBO-*m*-FPO was improved to 7.3% with the J_{sc} from 11.3 to 12.8 mA cm^{-2}, FF from 58% to 65%. However, for the PBO-*p*-FPO based device, the best weight ratio of PBO-*p*-FPO and $PC_{71}BM$ was 1:1. Incorporation of 3% DIO as additive leads to simultaneous enhancement in V_{oc} (0.86 to 0.93 V), J_{sc} (6.4 to 8.7 mA cm^{-2}) and FF (50% to 53%), resulting in PCE improvement from 2.8% to 4.3%. After Ca was substituted by ZrAcac film, the PCEs of PBO-*m*-FPO and PBO-*p*-FPO were improved *ca.* 10% (8.0% vs 7.3%) and 19% (5.1% vs 4.3%), respectively, under 3% DIO additive conditions. The key device parameters are shown in Table 3, and all the photovoltaic curves are exhibited in Figure S11 and related data with different conditions are concluded in Table S3. The external quantum efficiency (EQE) was measured to verify the accuracy of the above devices and the typical EQE curves are shown in Figure 3b. All the devices showed a high incident photon-to-electron conversion efficiency (IPCE) with a broad response from 300 to 700 nm. The PSCs derived from PBO-*m*-FPO showed a high IPCE compared to PBO-*p*-FPO, resulting in a higher J_{sc} values as well. The J_{sc} values of all the devices integrated from the EQE curves are rather consistent (less than 5% error) with the values obtained by J−V measurements.

There has been an intensive search for inverted device because of its long-term ambient stability. High hole mobility and energy level alignment of the low bandgap materials was successfully applied to roll-to-roll processing of inverted PSCs devices by Krebs et al. In such an inverted configuration, ZnO was employed as the electron selective layer due to its high

DOI: 10.1021/acs.macromol.5b00564
Macromolecules 2015, 48, 4347−4356

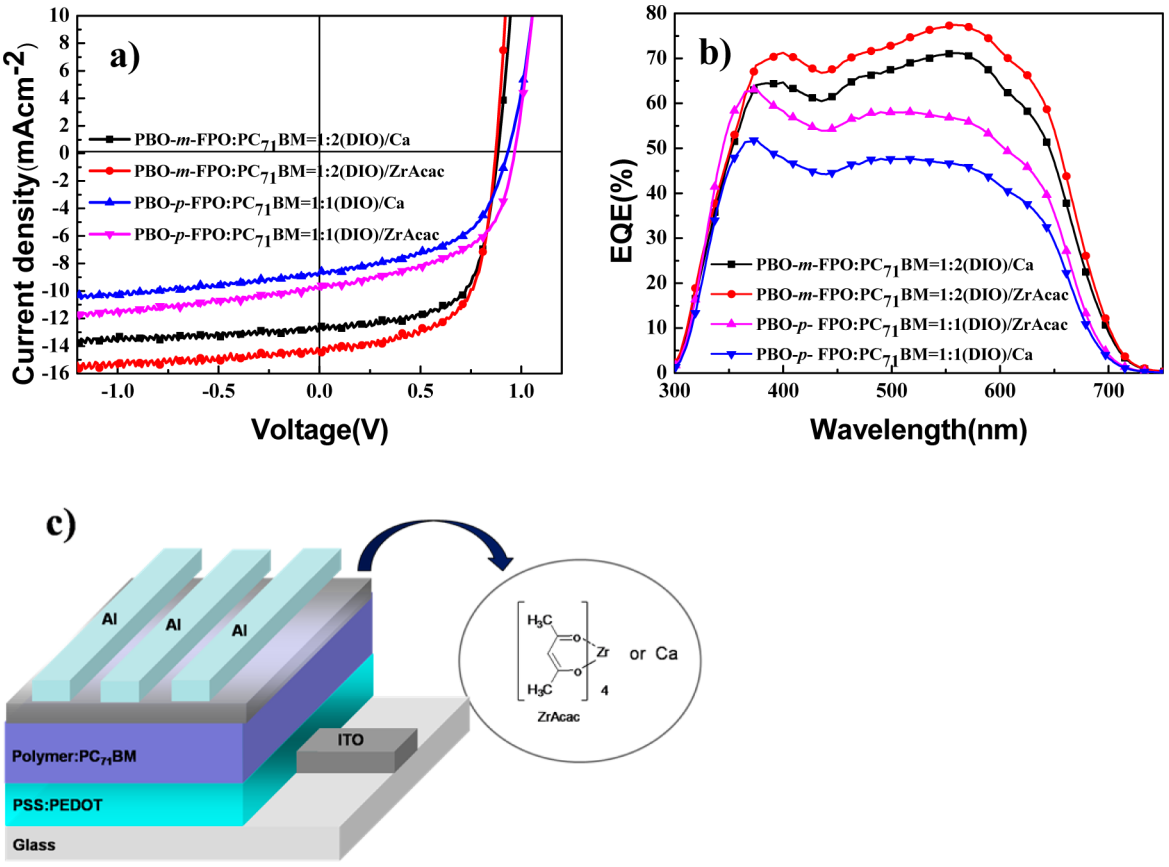

Figure 3. (a) J–V curves of the PSCs based on PBO-*m*-FPO:$PC_{71}BM$ (1:2, w/w) and PBO-*p*-FPO:$PC_{71}BM$ (1:1, w/w), under illumination of AM 1.5, 100 mW/cm^2. (b) EQE spectra of PSCs based on PBO-*m*-FPO:$PC_{71}BM$ (1:2, w/w) and PBO-*p*-FPO:$PC_{71}BM$ (1:1, w/w). (c) Device configuration of the polymers:$PC_{71}BM$ solar cell.

Table 3. Photovoltaic Data and the Device Parameter Standard Deviation of PSCs Based on PBO-*m*-FPO and PBO-*p*-FPO Blended with $PC_{71}BM$ with Different Cathode (the Average Values for 20 Devices in the Brackets) under the Illumination of AM 1.5G, 100 mW cm^{-2}

active layer	Ca/Al	ZrAcac/Al	V_{oc} (V)	J_{sc} (mA cm^{-2})	FF (%)	PCE (%)
PBO-*m*-FPO:$PC_{71}BM$ = 1:2	√		0.89	11.3	58	5.9 [5.6]
			(0.87 ± 0.02)	(10.9 ± 0.5)	(59 ± 1)	
PBO-*m*-FPO:$PC_{71}BM$ = 1:2 (3% DIO)	√		0.88	12.8	65	7.3 [7.1]
			(0.88 ± 0.01)	(12.6 ± 0.3)	(64 ± 1)	
PBO-*m*-FPO:$PC_{71}BM$ = 1:2 (3% DIO)		√	0.87	14.3	64	8.0 [7.9]
			(0.88 ± 0.01)	(14.2 ± 0.1)	(63 ± 2)	
PBO-*p*-FPO:PC71BM = 1:1	√		0.86	6.4	50	2.8 [2.5]
			(0.85 ± 0.01)	(5.9 ± 0.5)	(51 ± 1)	
PBO-*p*-FPO:PC71BM = 1:1 (3% DIO)	√		0.93	8.7	53	4.3 [4.1]
			(0.90 ± 0.03)	(8.7 ± 0.2)	(52 ± 1.5)	
PBO-*p*-FPO:PC71BM = 1:1 (3% DIO)		√	0.97	9.9	53	5.1 [5.0]
			(0.95 ± 0.02)	(10 ± 0.1)	(53 ± 1)	

electron mobility when inserted between ITO and the active layer.[42] However, owing to the poor electrical coherence at the organic and inorganic interface, the efficiency of invented device of PSCs is unsatisfactory. Hsu's group reported a cross-linkable fullerene material, [6,6]-phenyl-C61-butyric styryl dendron ester (PCBSD), which could enhance charge generation and direct electron transport pathways without causing interfacial erosion.[43,44] An inverted solar cell device based on ITO/ZnO/PCBSD/poly(3-hexylthiophene)-(P3HT):$PC_{60}BM$/MoO_3/Ag configuration as a control device achieved a PCE of 3.4%. The high efficiency based on PBO-*m*-FPO indicated us to fabricate PBO-*m*-FPO-based inverted PSCs, which active layer was changed from P3HT:$PC_{61}BM$ to PBO-*m*-FPO:$PC_{71}BM$ (1:2, w:w, 3% DIO), a high PCE of 6.3% with V_{oc} = 0.88 V, J_{sc} = 10.76 mA cm^{-2}, and FF = 67% was obtained. The structure of inverted device is shown in Figure S12 and all of the inverted device performances are summarized in Tables S4.

We can identify three possible reasons for difference in generated J_{sc} and FF between PBO-*m*-FPO and PBO-*p*-FPO with 3% DIO additive in the conventional device geometry (ITO/PEDOT:PSS/active layer/Ca/Al), although of similar

DOI: 10.1021/acs.macromol.5b00564
Macromolecules 2015, 48, 4347–4356

absorption and energy level: (i) the morphology of the active layers, (ii) the efficiency of photocurrent generation, and (iii) the molecular packing orientation. In the following, we investigate these three aspects in detail with the purpose to clarify different photovoltaic performance.

Hole Mobility. High performance solar cells depends on the balance of hole and electron mobilities. To gain further insight, we measured the charge mobilities of polymers, which have direct effect on charge transport. The hole-only mobility in the photosensitive layers were measured by space charge limited current (SCLC) method with devices (ITO/PEDOT:PSS/polymer:$PC_{71}BM$/Au) to investigate the charge transport in PBO-*m*-FPO and PBO-*p*-FPO films.[45] For the hole-only devices, SCLC is described by

$$J_{SCLC} = \frac{9}{8}\varepsilon_o\varepsilon_r\mu_o\frac{(V - V_{bi})^2}{d^3}\exp\left[0.89\gamma\sqrt{\frac{V - V_{bi}}{d}}\right] \quad (1)$$

where J is the current density, ε_0 is the permittivity of free space, ε_r is the dielectric constant of the active layer, μ_0 is the zero-field mobility, d stands for the thickness of the device, and $V = V_{appl} - V_{bi}$, where V_{appl} is the applied potential and V_{bi} is the built-in potential. Figure 4 shows the $\ln(Jd^3/V^2)$ vs $(V/d)^{0.5}$

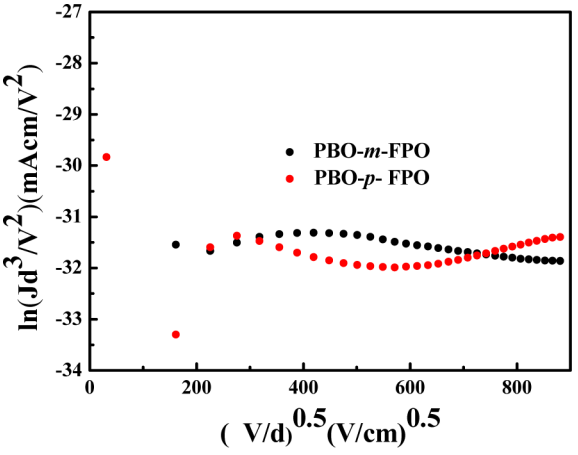

Figure 4. $\ln(Jd^3/V^2)$ vs $(V/d)^{0.5}$ plots of the blends of PBO-*m*-FPO/$PC_{71}BM$ and PBO-*p*-FPO/$PC_{71}BM$ for hole mobilities measurement by SCLC method.

plots. The hole mobilities of PBO-*m*-FPO and PBO-*p*-FPO were evaluated to be 2.7×10^{-4} and 1.6×10^{-5} $cm^2 \cdot V^{-1} \cdot s^{-1}$, respectively. When using the same method, we calculated previous reported similar nonfluorinated polymer (PBDTPO–DTBO) with a hole mobility of 1.1×10^{-4} $cm^2 \cdot V^{-1} \cdot s^{-1}$, which was a slightly lower than that of PBO-*m*-FPO but higher than that of PBO-*p*-FPO. The efficiency of photocurrent generation depends on the balance between charge carrier generation, recombination and transport.[46] At the same time, these factors especially charge recombination and transport can be affected from the hole and electron mobilities. The electron mobilities of two polymers are shown in Figure.S9 (Supporting Information). The electron mobility of PBO-*m*-FPO was evaluated to be 1.2×10^{-4} $cm^2 \cdot V^{-1} \cdot s^{-1}$ And the electron mobility of PBO-*p*-FPO was evaluated to be $8.0 \times 10^{-5} cm^2 \cdot V^{-1} \cdot s^{-1}$. The higher and balanced of hole and electron mobilities of PBO-*m*-FPO (2.7×10^{-4} $cm^2 \cdot V^{-1} \cdot s^{-1}$ for hole-only and 1.2×10^{-4} $cm^2 \cdot V^{-1} \cdot s^{-1}$ for electron-only) will contribute to the higher efficiency of photocurrent generation.

Field-effect mobilities give a valuable insight into the quality of the charge carrier transport. Thus, top-gate/bottom-contact (TG/BC) gate field-effect transistors (FETs) devices were fabricated to measure their hole mobilities of polymers.[47] The active layers were spin-coated from *o*-dichlorobenzene (8 mg/mL) onto octadecyltrichlorosilane (OTS) treated SiO_2/Si substrate and Au was evaporated as the source/drain electrodes, which were subsequently annealed for 1 h at 150 °C according to Li group's work.[48] The typical output and transfer curves of the PBO-*m*-FPO and PBO-*p*-FPO at annealing 150 °C are depicted in Figure S10a,b . For the direct spin-coated films, all polymers show mobilities with $\mu \approx 10^{-3}$–10^{-5} $cm^2 \cdot V^{-1} \cdot s^{-1}$ (2.37×10^{-3} $cm^2 \cdot V^{-1} \cdot s^{-1}$ for PBO-*m*-FPO, 2.47×10^{-5} $cm^2 \cdot V^{-1} \cdot s^{-1}$ for PBO-*p*-FPO). However, after annealing at 150 °C, they exhibited μ up to 1.72×10^{-2} and 1.32×10^{-2} $cm^2 \cdot V^{-1} \cdot s^{-1}$ for PBO-*m*-FPO and PBO-*p*-FPO, respectively, which is likely due to improved molecular packing with thermal annealing.

Morphological Characterization of BHJ Films. To better understand the origin of the differences in PCE, the morphology of the optimized photoactive layer was examined by the atomic force microscopy (AFM) and transmission electron microscopy (TEM), as well as Grazing-incidence wide-angle X-ray scattering (GIWAXS). From Figure 5, the height and phase images of the surface were investigated by AFM for the blend films processed without or with 3% DIO additive. The surface of PBO-*m*-FPO:$P_{71}CBM$ (1:2) film obtained without DIO shows a root-mean-square (RMS) roughness of 2.11 nm (Figure 5a), which is lower than that (5.32 nm) of the 3% DIO treatment as shown in Figure 5b. Similar to PBO-*m*-FPO, in the case of 3% DIO, the RMS based on PBO-*p*-FPO blend $PC_{71}BM$ (1:1) increased from 0.68 to 3.68 nm shown in Figure 5, parts c and d. The above AFM results revealed that the addition of DIO additive led to enhanced aggregation of the polymers and fullerene in the active layer, which is favorable for charge separation/transport and thus.[49] In TEM images(Figure 6), the bright regions were polymers-rich and the dark regions were PCBM-rich. Obviously, the fibril width becomes smaller after with 3% DIO treatment (Figure 6a–d). The larger crystalline fibril limited the charge generation. The TEM images for polymer/$PC_{71}BM$ with or without DIO are fully consistent with the results of photovoltaic data. Wider fibrils may form longer pathways, which will not benefit the excition transport and separation that occurs at the interface of donor and acceptor. On the other hand, the fibril width sizes of Figure 6, parts a and c, may in part be larger than exciton diffusion lengths (*ca.* 10 nm), so the photogenerated excitons will be partly recombined before reaching the interfaces of the donor and acceptor, resulting in relatively poorer exciton separation efficiency and lower current density.[50]

Grazing-incidence wide-angle X-ray scattering (GIWAXS) was also used to gain insight into the structural differences of the pure polymer and blend films. Figures 7 and 8 show GIWAXS patterns and line profiles of pure polymer and polymer:$PC_{71}BM$ blend films prepared from ODCB solutions with or without DIO. The molecular packing orientation can be deduced from the GIWAXS patterns, where the molecular packing out-of-plane appears nominally along the q_z axis and the in-plane ordering along the q_{xy}. Comparison with pristine PBO-*p*-FPO film, the intensity of the π–π stacking peak (010) of pure PBO-*m*-FPO ($q = 1.70$ Å^{-1}, $d = 3.69$ Å) is more intense in the out-of-plane direction (Figure 7a,d and Figure 8). The pronounced (010) peak at the out-of-plane direction indicates there is a preponderance of the face-on orientation. The (010)

DOI: 10.1021/acs.macromol.5b00564
Macromolecules 2015, 48, 4347–4356

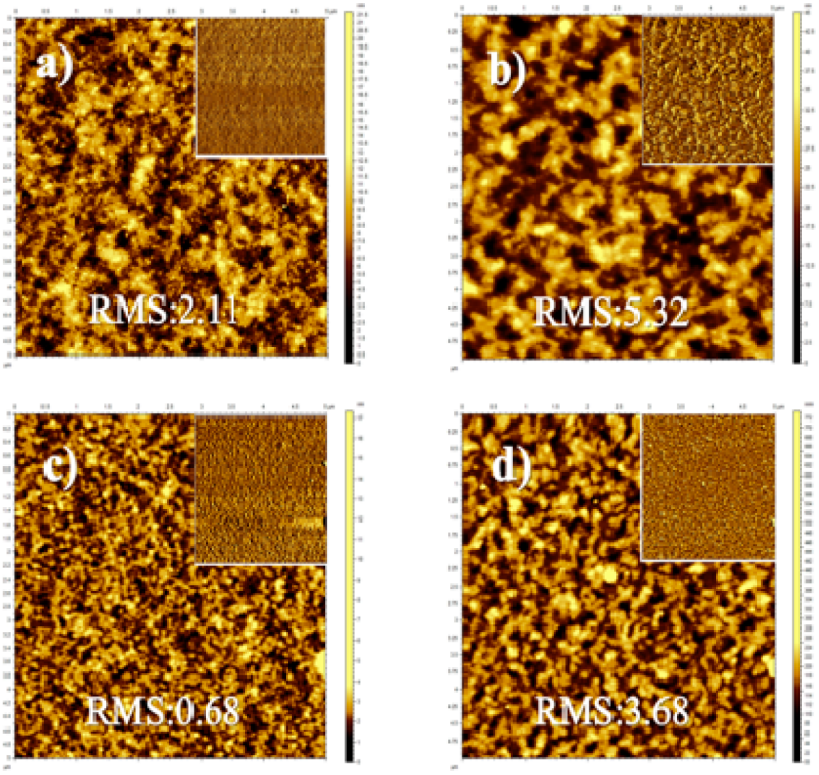

Figure 5. AFM images (5 μm × 5 μm) of PBO-*m*-FPO:$PC_{71}BM$(1:2, w/w) blend film on ITO/PEDOT:PSS substrate without (a) and with (b) 3% DIO and AFM images (5 μm × 5 μm) of PBO-*p*-FPO:$PC_{71}BM$(1:1, w/w) blend film on ITO/PEDOT:PSS substrate without (c) and with (d) 3% DIO. Insets are phase images of 5 μm × 5 μm size.

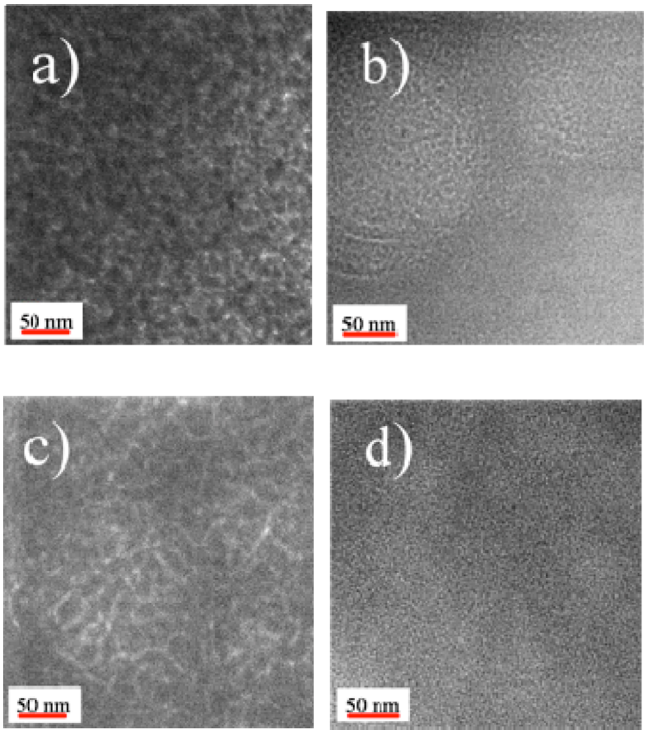

Figure 6. TEM images of polymer: $PC_{71}BM$ blend films: a) PBO-*m*-FPO: $PC_{71}BM$ without DIO, b) PBO-*m*-FPO: $PC_{71}BM$ with 3% DIO, c) PBO-*p*-FPO: $PC_{71}BM$ without DIO, d) PBO-*p*-FPO: $PC_{71}BM$ with 3% DIO.

coherence length (calculated by Scherrer equation)[51] of PBO-*m*-FPO and PBO-*p*-FPO pure film are 3.4 and 2.5 nm. These results demonstrate that PBO-*m*-FPO showing better $\pi-\pi$ stacking ordering. The "face-on" $\pi-\pi$ stacking of donor polymers in the active layer is more favorable for charge transport than "edge-on" stacking.[17] However, when the $PC_{71}BM$ is added, all the (010) peaks in the blend (with or without DIO) are disappeared, which suggests that the $\pi-\pi$ packing is not well ordered. It should also be noted that the lamellar packing peak (100) of PBO-*m*-FPO pure film is weak. When it is blended with $PC_{71}BM$, (100) peak becomes more pronounced, particularly in in-plane direction. Further processing treatment with DIO induces even stronger (100) peak for PBO-*m*-FPO:$PC_{71}BM$ blend. However, the *p*-fluorinated polymer (Figure 7d) shows relatively weak (010) reflection along the Q_z axes, which implies that the intermolecular interaction between adjacent polymer chains are restricted, mainly because of the *m*-alkoxy side chains. When it is blended with fullerene, both (100) and (010) become weaker, which is different from PBO-*m*-FPO system. In general, stronger (100) and (010) peaks and higher order peaks for PBO-*m*-FPO pure film and blend film indicate the presence of the higher polymer crystallites degree.[52,53] The highly ordered structure will induce purer domains that would reduce bimolecular recombination.[22,54,55] This explains why PBO-*m*-FPO based devices show higher FF and J_{sc}.

■ CONCLUSIONS

In summary, we have reported two similar low bandgap conjugated polymers with fluorine atom on *m*- and *p*-phenyl substituted BDT units. The morphology, hole mobility, and molecular packing demonstrated a large difference, resulting in obviously different device performance. However, the optical properties and molecular energy levels remained almost the

DOI: 10.1021/acs.macromol.5b00564
Macromolecules 2015, 48, 4347−4356

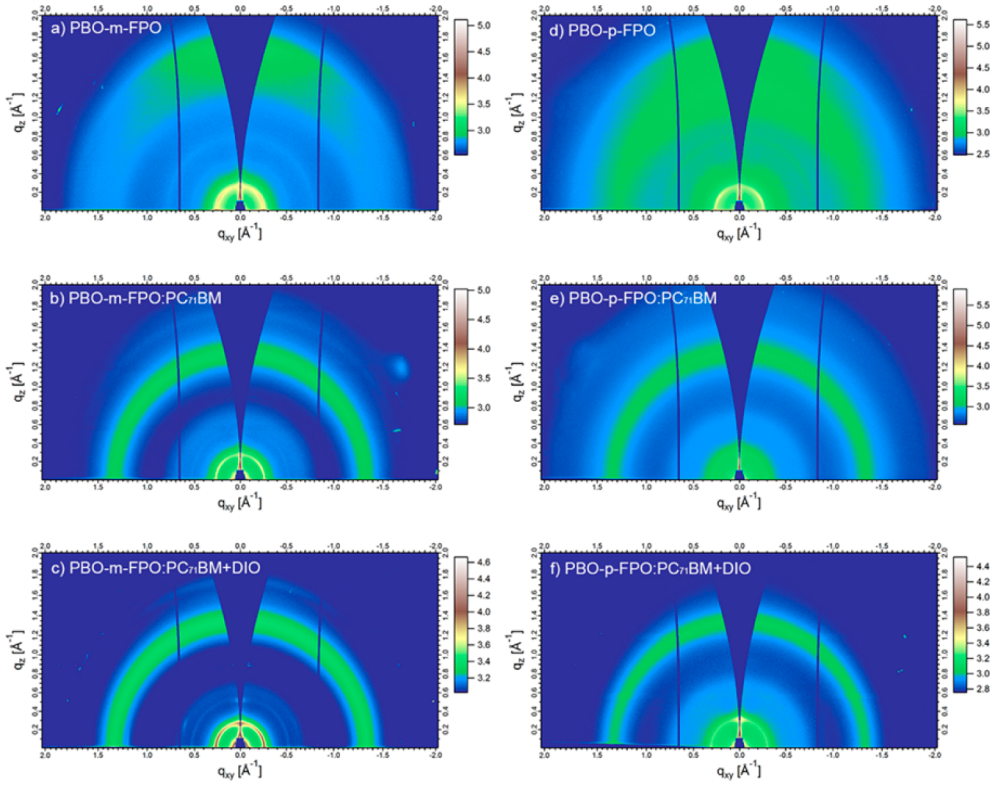

Figure 7. Grazing incidence wide-angle X-ray scattering diffraction (GIWAXS) pattern of (a, d) pure PBO-*m*-FPO and PBO-*p*-FPO and (b, e) PBO-*m*-FPO:$PC_{71}BM$ and PBO-*p*-FPO:$PC_{71}BM$ blend films without DIO and (c, f) with DIO.

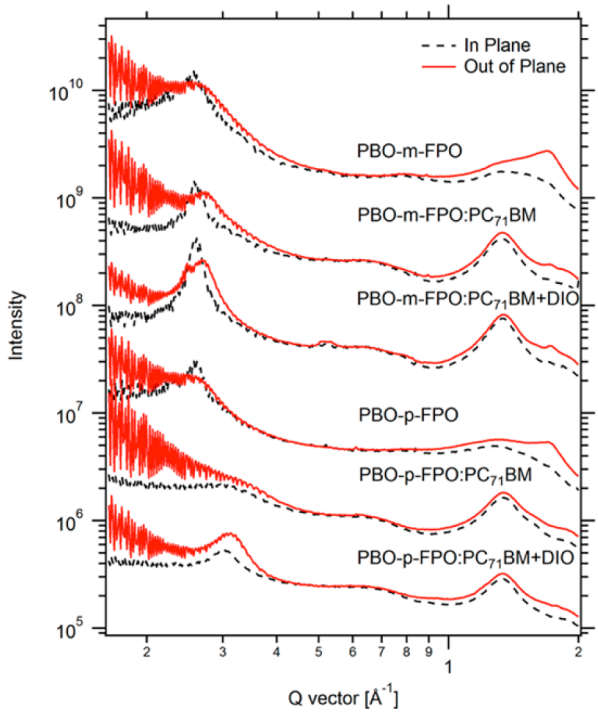

Figure 8. Line profiles (in-plane and out-of-plane) of grazing incidence wide-angle X-ray scattering diffraction (GIWAXS) for pure and blend films.

same. When 3% DIO was selected as active layer additive, the better phase separation could be found from AFM and TEM. With the low workfunction and insensitive to environmental moisture and oxygen ZrAcac/Al substituting Ca/Al under the 3% DIO condition, the PCE of PBO-*m*-FPO and PBO-*p*-FPO were increased by ca. 10% (8.0% vs 7.3%) and 19% (5.1% vs 4.3%), respectively, under the illumination of AM 1.5, 100 mW cm^{-2}. Our findings indicate that the introduction of fluorine atom may promote the photovoltaic performance, but incorporation onto the different positions can exert great effects on the optoelectronic properties.

EXPERIMENTAL SECTION

Characterization. ^1H NMR spectra were recorded using a Bruker AV-500 spectrometer in deuterated chloroform solution at 298 K, unless specified otherwise. Chemical shifts were reported as δ values (ppm) with tetramethylsilane (TMS) as the internal reference. Molecular weight and polydispersity of the polymers were determined by gel permeation chromatography (GPC) analysis with polystyrene as standard (Waters 515 HPLC pump, a Waters 2414 differential refractometer, and three Waters Styragel columns (HT2, HT3, and HT4)) using THF (HPLC grade) as eluent at a flow rate of 1.0 mL/min at 35 °C. Thermogravimetric analysis (TGA) was conducted on a PerkinElmer TGA-7 with a heating rate of 20 K/min under nitrogen atmosphere. UV−vis absorption spectra were recorded on the SHIMADZU UV-2450 spectrophotometer. For the solid state measurements, polymer solution in chloroform was spin-coated on quartz plates. The cyclic voltammetry was recorded with a computer controlled Zahner IM6e electrochemical workstation using polymer films on carbon electrode (1.0 cm^2) as the working electrode, a platinum wire as the counter electrode and Ag/AgCl (0.1 M) as the reference electrode in an anhydrous and argon-saturated solution of 0.1 M of tetrabutylammonium hexafluorophosphate (Bu_4NPF_6) in acetonitrile at a scanning rate of 50 $mV{\cdot}s^{-1}$. Electrochemical onsets were determined at the position where the current starts to differ from the baseline. Hole field effect mobility of the polymer was measured by using OFET method performed on Keithley 4200 SCS semiconductor parameter analyzer. The morphologies of the polymer/$PC_{71}BM$ blend films were investigated by atomic force microscopy (AFM, Agilent

DOI: 10.1021/acs.macromol.5b00564
Macromolecules 2015, 48, 4347−4356

Technologies, 5500 AFM/SPM System, USA) in contacting mode with a 5 μm scanner. Transmission electron microscope (TEM) measurements were performed in a JEM-2100F. GIWAXS, were performed at beamline 7.3.3,[55,56] respectively at the Advanced Light Source, Lawrence Berkeley National Laboratory, Berkeley, CA.

Fabrication and Characterization of Polymer Solar Cells. The PSCs were fabricated in the configuration of the traditional sandwich structure with an indium tin oxide (ITO) glass positive electrode and a Ca/Al (or ZrAcac/Al) negative electrode. Patterned ITO glass with a sheet resistance of 10 Ω/sq was purchased from CSG HOLDING Co. Ltd. (China). The ITO glass was cleaned by sequential ultrasonic treatment in detergent, deionized water, acetone and isopropanol, and then treated in an ultraviolet-ozone chamber (Ultraviolet Ozone Cleaner, Jelight Company, USA) for 20 min. Then PEDOT:PSS (poly(3,4-ethylene dioxythiophene): poly(styrenesulfonate)) (Baytron PVP Al 4083, Germany) was filtered through a 0.45 μm poly(tetrafluoroethylene) (PTFE) filter and spin coated at 3000 rpm for 40 s on the ITO substrate. Subsequently, PEDOT: PSS film was baked at 150 °C for 15 min in the air, and the thickness of the PEDOT:PSS layer is about 40 nm. The polymers and $PC_{71}BM$ (10 mg/mL for polymers) were dissolved in ODCB and 3% volume ratio of 1,8-diiodooctane (DIO, Sigma-Aldrich) overnight and spin-cast at 1700 rpm for 90 s onto the PEDOT:PSS layer. The thickness of the photoactive layer is about 110 nm measured by Ambios Technology XP-2 profilometer. A bilayer cathode consisting of Ca (~15 nm) capping with Al (~40 nm) was thermal evaporated under a shadow mask with a base pressure of ca. 10^{-5} Pa. The active area of the PSCs is 5 mm^2. The ZrAcac (J&K, China) was simply prepared by spin-coating its ethanol solution (1 mg mL^{-1}) on a photoactive layer at 3000 rpm for 30 s at room temperature; no thermal annealing or any other post-treatment was performed. Finally, top electrodes were deposited in a vacuum onto the active layer.The active area of the device was 5 mm^2.

For the fabrication of inverted cells, zinc acetate dihydrate (purchased from Sigma-Aldrich) was dissolved in 2-methoxyenthanol (10 mg mL^{-1}) and small amount of ethanolamine. The obtained solution was spin-casted on precleaned ITO substrates and baked at 180 °C for 10 min in the air to form the ZnO layer with thickness of 40 nm. [6,6]-Phenyl-C61-butyric styryl dendron ester (PCBSD) was dissolved in *o*-dichlorobenzne (ODCB) to reach a concentration of 0.5 wt %. The PCBSD solution was spin-casted onto the ZnO layer to form a thin film with a thickness of ca. 10 nm. Subsequently, the film was annealed at 180 °C for 10 min in the glovebox for thermal cross-linking. The polymer PBO-*m*-FPO was dissolved in ODCB (0.77 wt %), and $PC_{71}BM$ was then added into the solution to reach the desired weight ratio. The solution was stirred at 70 °C for overnight and filtrated through a 0.45 um filter. Before spin-casting the active layer, the solution was mixed with 3 vol % DIO. Then, the active layers were then spin-coated on the top of C-PCBSD layer to reached desired thickness. Finally, the anode made of MoO_3 (6 nm) and Ag (150 nm) was evaporated through a shadow mask under vacuum (<10^{-6} Torr). Each sample consists of four independent pixels defined by an active area of 0.04 cm^2.

Device characterization was carried out under AM 1.5G irradiation with the intensity of 100 mW cm^{-2} (Oriel 67005, 500 W), calibrating by a standard silicon cell. *J*−*V* curves were recorded with a Keithley 236 digital source meter. A xenon lamp with AM 1.5 filter was used as the white light source and the optical power was 100 mW cm^{-2}. The EQE measurements of PSCs were performed by Stanford Systems model SR830 DSP lock-in amplifier coupled with WDG3 monochromator and 500 W xenon lamp. A calibrated silicon detector was used to determine the absolute photosensitivity at different wavelengths. All of these fabrications and characterizations after cleaning of ITO substrates were conducted in a glovebox.

■ ASSOCIATED CONTENT

Supporting Information

Experimental details, monomer synthesis (Scheme S1, showing synthetic routes), H NMR spectra (Figures S1−S6), TGA, calculated HOMO and LUMO levels of new moieties, electron mobilities of two polymers, field transistor behaviors, *J*−*V* curves and inverted device geometry of polymers:$PC_{71}BM$ (Figures S7−S12, respectively), optical and electrochemical data (Table S1), and field transistor behavior characteristics and conventional and inverted photovoltaic data (Tables S2−S4). The Supporting Information is available free of charge on the ACS Publications website at DOI: 10.1021/acs.macromol.5b00564.

■ AUTHOR INFORMATION

Corresponding Authors

*E-mail: yingpingzou@csu.edu.cn (Y.Z.).
*E-mail: cshsu@mail.nctu.edu.tw (C.-S.H.).
*E-mail: wma5@ncsu.edu (W.M.).

Notes

The authors declare no competing financial interest.

■ ACKNOWLEDGMENTS

This work was supported by NSFC (Nos. 51173206, 21161160443) and Central South University. X-ray data was acquired at beamlines 7.3.3 at the Advanced Light Source,[55,56] which is supported by the Director, Office of Science, Office of Basic Energy Sciences, of the U.S. Department of Energy under Contract No. DE-AC02-05CH11231

■ REFERENCES

(1) Dennler, G.; Scharber, M. C.; Brabec, C. J. *Adv. Mater.* **2009**, *21*, 1323−1338.
(2) Ye, L.; Zhang, S.; Zhao, W.; Yao, H.; Hou, J. *Chem. Mater.* **2014**, *26*, 3603−3605.
(3) Cui, C.; Wong, W.-Y.; Li, Y. *Energy Environ. Sci.* **2014**, *7*, 2276.
(4) Nguyen, T. L.; Choi, H.; Ko, S.-J.; Uddin, M. A.; Walker, B.; Yum, S.; Jeong, J.-E.; Yun, M. H.; Shin, T.; Hwang, S. *Energy Environ. Sci.* **2014**, *7*, 3040−3051.
(5) Liu, Y.; Zhao, J.; Li, Z.; Mu, C.; Ma, W.; Hu, H.; Jiang, K.; Lin, H.; Ade, H.; Yan, H. *Nat. Commun.* **2014**, *5*, 5293.
(6) Li, Y. *Acc. Chem. Res.* **2012**, *45*, 723−733.
(7) Günes, S.; Neugebauer, H.; Sariciftci, N. S. *Chem. Rev.* **2007**, *107*, 1324−1338.
(8) Park, H. J.; Kang, M. G.; Ahn, S. H.; Guo, L. J. *Adv. Mater.* **2010**, *22*, E247−53.
(9) Chen, L. M.; Hong, Z.; Li, G.; Yang, Y. *Adv. Mater.* **2009**, *21*, 1434−1449.
(10) Peet, J.; Senatore, M. L.; Heeger, A. J.; Bazan, G. C. *Adv. Mater.* **2009**, *21*, 1521−1527.
(11) Kan, B.; Zhang, Q.; Li, M.; Wan, X.; Ni, W.; Long, G.; Wang, Y.; Yang, X.; Feng, H.; Chen, Y. *J. Am. Chem. Soc.* **2014**, *136*, 15529−32.
(12) Shin, H. J.; Kim, K. K.; Benayad, A.; Yoon, S. M.; Park, H. K.; Jung, I. S.; Jin, M. H.; Jeong, H. K.; Kim, J. M.; Choi, J. Y. *Adv. Funct Mater.* **2009**, *19*, 1987−1992.
(13) Roncali, J. *Acc. Chem. Res.* **2009**, *42*, 1719−1730.
(14) Li, Y.; Zou, Y. *Adv. Mater.* **2008**, *20*, 2952−2958.
(15) Li, G.; Shrotriya, V.; Huang, J.; Yao, Y.; Moriarty, T.; Emery, K.; Yang, Y. *Nat. Mater.* **2005**, *4*, 864−868.
(16) Wang, N.; Chen, Z.; Wei, W.; Jiang, Z. *J. Am. Chem. Soc.* **2013**, *135*, 17060−8.
(17) Kim, J.-H.; Shin, S. A.; Park, J. B.; Song, C. E.; Shin, W. S.; Yang, H.; Li, Y.; Hwang, D.-H. *Macromolecules* **2014**, *47*, 1613−1622.
(18) Li, G.; Kang, C.; Gong, X.; Zhang, J.; Li, C.; Chen, Y.; Dong, H.; Hu, W.; Li, F.; Bo, Z. *Macromolecules* **2014**, *47*, 4645−4652.
(19) Peng, Q.; Liu, X.; Su, D.; Fu, G.; Xu, J.; Dai, L. *Adv. Mater.* **2011**, *23*, 4554−8.
(20) Xiao, L.; Liu, B.; Chen, X.; Li, Y.; Tang, W.; Zou, Y. *RSC Adv.* **2013**, *3*, 11869.

DOI: 10.1021/acs.macromol.5b00564
Macromolecules 2015, 48, 4347−4356

(21) You, J.; Dou, L.; Yoshimura, K.; Kato, T.; Ohya, K.; Moriarty, T.; Emery, K.; Chen, C. C.; Gao, J.; Li, G.; Yang, Y. *Nat. Commun.* **2013**, *4*, 1446.
(22) Albrecht, S.; Janietz, S.; Schindler, W.; Frisch, J.; Kurpiers, J.; Kniepert, J.; Inal, S.; Pingel, P.; Fostiropoulos, K.; Koch, N.; Neher, D. *J. Am. Chem. Soc.* **2012**, *134*, 14932−44.
(23) Kim, B.-G.; Jeong, E. J.; Chung, J. W.; Seo, S.; Koo, B.; Kim, J. *Nat. Mater.* **2013**, *12*, 659−664.
(24) Wang, Y.; Parkin, S. R.; Gierschner, J.; Watson, M. D. *Org. Lett.* **2008**, *10*, 3307−3310.
(25) Yang, L.; Tumbleston, J. R.; Zhou, H.; Ade, H.; You, W. *Energy Environ. Sci.* **2013**, *6*, 316.
(26) Zhou, H.; Yang, L.; Stuart, A. C.; Price, S. C.; Liu, S.; You, W. *Angew. Chem.* **2011**, *123*, 3051−3054.
(27) Carsten, B.; Szarko, J. M.; Son, H. J.; Wang, W.; Lu, L.; He, F.; Rolczynski, B. S.; Lou, S. J.; Chen, L. X.; Yu, L. *J. Am. Chem. Soc.* **2011**, *133*, 20468−75.
(28) Zhang, M.; Guo, X.; Zhang, S.; Hou, J. *Adv. Mater.* **2014**, *26*, 1118−23.
(29) Lei, T.; Xia, X.; Wang, J. Y.; Liu, C. J.; Pei, J. *J. Am. Chem. Soc.* **2014**, *136*, 2135−41.
(30) Liu, B.; Chen, X.; Zou, Y.; Xiao, L.; Xu, X.; He, Y.; Li, L.; Li, Y. *Macromolecules* **2012**, *45*, 6898−6905.
(31) Ding, P.; Zhong, C.; Zou, Y.; Pan, C.; Wu, H.; Cao, Y. *J. Phys. Chem. C* **2011**, *115*, 16211−16219.
(32) Yuan, J.; Xiao, L.; Liu, B.; Li, Y.; He, Y.; Pan, C.; Zou, Y. *J. Mater. Chem. A* **2013**, *1*, 10639−10645.
(33) Qin, R.; Li, W.; Li, C.; Du, C.; Veit, C.; Schleiermacher, H.-F.; Andersson, M.; Bo, Z.; Liu, Z.; Inganäs, O. *J. Am. Chem. Soc.* **2009**, *131*, 14612−14613.
(34) Jo, J. W.; Jung, J. W.; Wang, H.-W.; Kim, P.; Russell, T. P.; Jo, W. H. *Chem. Mater.* **2014**, *26*, 4214−4220.
(35) Wu, J.-S.; Jheng, J.-F.; Chang, J.-Y.; Lai, Y.-Y.; Wu, K.-Y.; Wang, C.-L.; Hsu, C.-S. *Polym. Chem.* **2014**, *5*, 6472−6479.
(36) Liu, M.; Liang, Y.; Chen, P.; Chen, D.; Liu, K.; Li, Y.; Liu, S.; Gong, X.; Huang, F.; Su, S.-J.; Cao, Y. *J. Mater. Chem. A* **2014**, *2*, 321.
(37) Valiev, M.; Bylaska, E. J.; Govind, N.; Kowalski, K.; Straatsma, T. P.; Van Dam, H. J.; Wang, D.; Nieplocha, J.; Apra, E.; Windus, T. L. *Comput. Phys. Commun.* **2010**, *181*, 1477−1489.
(38) Liu, B.; Najari, A.; Pan, C.; Leclerc, M.; Xiao, D.; Zou, Y. *Macromol. Rapid Commun.* **2010**, *31*, 391−398.
(39) Blouin, N.; Michaud, A.; Gendron, D.; Wakim, S.; Blair, E.; Neagu-Plesu, R.; Belletête, M.; Durocher, G.; Tao, Y.; Leclerc, M. *J. Am. Chem. Soc.* **2008**, *130*, 732−742.
(40) He, Z.; Zhong, C.; Huang, X.; Wong, W. Y.; Wu, H.; Chen, L.; Su, S.; Cao, Y. *Adv. Mater.* **2011**, *23*, 4636−43.
(41) Tan, Z.; Li, S.; Wang, F.; Qian, D.; Lin, J.; Hou, J.; Li, Y. *Sci. Rep* **2014**, *4*, 4691.
(42) Sun, Y.; Seo, J. H.; Takacs, C. J.; Seifter, J.; Heeger, A. J. *Adv. Mater.* **2011**, *23*, 1679−83.
(43) Chang, C. Y.; Wu, C. E.; Chen, S. Y.; Cui, C.; Cheng, Y. J.; Hsu, C. S.; Wang, Y. L.; Li, Y. *Angew. Chem., Int. Ed. Engl.* **2011**, *50*, 9386−90.
(44) Cheng, Y.-J.; Cao, F.-Y.; Lin, W.-C.; Chen, C.-H.; Hsieh, C.-H. *Chem. Mater.* **2011**, *23*, 1512−1518.
(45) Chen, C.-H.; Cheng, Y.-J.; Chang, C.-Y.; Hsu, C.-S. *Macromolecules* **2011**, *44*, 8415−8424.
(46) Mihailetchi, V.; Wildeman, J.; Blom, P. *Phys. Rev. Lett.* **2005**, 94.
(47) Lenes, M.; Morana, M.; Brabec, C. J.; Blom, P. W. M. *Adv. Funct Mater.* **2009**, *19*, 1106−1111.
(48) Xu, X.; Liu, B.; Zou, Y.; Guo, Y.; Li, L.; Liu, Y. *Adv. Funct Mater.* **2012**, *22*, 4139−4148.
(49) Li, W.; Zhou, Y.; Viktor Andersson, B.; Mattias Andersson, L.; Thomann, Y.; Veit, C.; Tvingstedt, K.; Qin, R.; Bo, Z.; Inganäs, O.; Würfel, U.; Zhang, F. *Org. Electron.* **2011**, *12*, 1544−1551.
(50) Li, W.; Hendriks, K. H.; Furlan, A.; Roelofs, W. S.; Wienk, M. M.; Janssen, R. A. *J. Am. Chem. Soc.* **2013**, *135* (50), 18942−8.
(51) Smilgies, D.-M. *J. Appl. Crystallogr.* **2009**, *42*, 1030.
(52) Perez, L. A.; Rogers, J. T.; Brady, M. A.; Sun, Y.; Welch, G. C.; Schmidt, K.; Toney, M. F.; Jinnai, H.; Heeger, A. J.; Chabinyc, M. L.; Bazan, G. C.; Kramer, E. J. *Chem. Mater.* **2014**, *26*, 6531−6541.
(53) Rivnay, J.; Mannsfeld, S. C.; Miller, C. E.; Salleo, A.; Toney, M. F. *Chem. Rev.* **2012**, *112*, 5488−519.
(54) Ma, W.; Tumbleston, J. R.; Wang, M.; Gann, E.; Huang, F.; Ade, H. *Adv. Energy Mater.* **2013**, *3*, 864−872.
(55) Ma, W.; Tumbleston, J. R.; Ye, L.; Wang, C.; Hou, J.; Ade, H. *Adv. Mater.* **2014**, *26*, 4234−41.
(56) Hexemer, A.; Bras, W.; Glossinger, J.; Schaible, E.; Gann, E.; Kirian, R.; MacDowell, A.; Church, M.; Rude, B.; Padmore, H. *J. Phys.: Conf. Ser.* **2010**, *247*, 012007.

DOI: 10.1021/acs.macromol.5b00564
Macromolecules 2015, 48, 4347−4356